



Article

Intercomparisons and Evaluations of Satellite-Derived Arctic Sea Ice Thickness Products

Feifan Chen ^{1,†}, Deshuai Wang ^{2,3,†}, Yu Zhang ^{1,4,*} , Yi Zhou ⁵ and Changsheng Chen ²

¹ College of Oceanography and Ecological Science, Shanghai Ocean University, Shanghai 201306, China; m220200673@st.shou.edu.cn

² School for Marine Science and Technology, University of Massachusetts Dartmouth, New Bedford, MA 02744, USA; wangd@umces.edu (D.W.); c1chen@umassd.edu (C.C.)

³ Horn Point Laboratory, University of Maryland Center for Environment Science, Cambridge, MD 21613, USA

⁴ Southern Marine Science and Engineering Guangdong Laboratory (Zhuhai), Zhuhai 519082, China

⁵ School of Oceanography, Shanghai Jiao Tong University, Shanghai 200030, China; yizhou.os@sjtu.edu.cn

* Correspondence: yuzhang@shou.edu.cn

† These authors contributed equally to this work.

Abstract: Currently, Arctic sea ice thickness (SIT) data with extensive spatiotemporal coverage primarily comes from satellite observations, including CryoSat-2, Soil Moisture and Ocean Salinity (SMOS), and the Ice, Cloud, and Land Elevation Satellite-2 (ICESat-2). The studies of the intercomparison and evaluation of multi-source satellite products in recent years are limited. In this study, three latest version products of ICESat-2, CryoSat-2, and CS2SMOS (a merged product of CryoSat-2 and SMOS) were examined from October to April, between 2018 and 2022. Three types of observation including airborne data from the Operation IceBridge (OIB) and IceBird, and in situ data from Beaufort Gyre Exploration Project (BGEF) are selected as the reference in the evaluation. The intercomparison results show that the mean SIT is generally largest in ICESat-2, second largest in CryoSat-2, and smallest in CS2SMOS. The SIT in CryoSat-2 is closer to the SIT in ICESat-2. The thickness displayed by the three satellite products starts to increase at different freezing months, varying between October and November. The three satellite products demonstrated the strongest agreements in SIT in the Beaufort Sea and Central Arctic regions, and exhibited the most distinct differences in the Barents Sea. In the evaluation with OIB data, three satellite-derived SIT were generally underestimated and CS2SMOS demonstrates the closest match. The evaluation using IceBird data indicates an underestimation for all satellites, with CryoSat-2 showing the best agreement. In the assessment with BGEF data, ICESat-2 displayed a more pronounced degree of overestimation or underestimation compared to the other two satellites, and CS2SMOS exhibited the optimal agreement. Based on the comprehensive consideration, CS2SMOS demonstrated the best performance with the airborne and in situ observational data, followed by CryoSat-2 and ICESat-2. The intercomparison and evaluation results of satellite products can contribute to a further understanding of the accuracies and uncertainties of the latest version SIT retrieval and the appropriate selection and utilization of satellite products.

Keywords: arctic; sea ice thickness; satellite; intercomparison; evaluation



Citation: Chen, F.; Wang, D.; Zhang, Y.; Zhou, Y.; Chen, C. Intercomparisons and Evaluations of Satellite-Derived Arctic Sea Ice Thickness Products. *Remote Sens.* **2024**, *16*, 508. <https://doi.org/10.3390/rs16030508>

Academic Editors: Mohammed Shokr and Yufang Ye

Received: 14 December 2023

Revised: 15 January 2024

Accepted: 26 January 2024

Published: 29 January 2024



Copyright: © 2024 by the authors. Licensee MDPI, Basel, Switzerland. This article is an open access article distributed under the terms and conditions of the Creative Commons Attribution (CC BY) license (<https://creativecommons.org/licenses/by/4.0/>).

1. Introduction

Arctic Sea ice, as an indicator of global climate change, plays a critical role in regulating the exchange of heat, moisture, and momentum between the atmosphere and the ocean [1–4]. The growth, transportation, and melting of sea ice can affect the seasonal balance of freshwater, thereby influencing Arctic water transports and thermohaline circulations [5,6]. The Arctic sea ice has significantly declined during the last decades [7], characterized by the retreat of sea ice extent and area [8], reduction of sea ice thickness (SIT) [9], and the acceleration of sea ice motion [10]. The reduction of Arctic sea ice has

enhanced the navigability of maritime transportation and shipping routes [11,12]. Different from sea ice concentration and sea ice drift, the available data of SIT are limited [13,14].

Currently, some different methods are employed for measuring SIT, including upward looking sonars (ULS), airborne missions, drill holes, and buoys [15–18]. However, these detection methods are difficult to achieve a relatively broad spatiotemporal coverage. Satellite-derived SIT products with high spatial resolution, large measurement range, and long time series, are widely applied in the studies of SIT [9,19,20]. In the past two decades, several satellites were launched and their SIT products are available. The Ice, Cloud, and Land Elevation Satellite (ICESat) with a precision laser altimeter system covers the period 2003–2008 [21]. The CryoSat-2 with synthetic aperture radar/Interferometric Radar Altimeter was carried out in 2010 [22]. The Soil Moisture and Ocean Salinity (SMOS) mission was launched in 2009 and the payload consists of the Microwave Imaging Radiometer using Aperture Synthesis (MIRAS) at an L-band frequency of 1.4 GHz [23]. The CS2SMOS SIT data product is a fusion of CryoSat-2 and SMOS data developed by Alfred Wegener Institute (AWI) and the University of Hamburg [24]. The Ice, Cloud, and Land Elevation Satellite-2 (ICESat-2) started to measure SIT in 2018 [25]. However, these products have measurement differences in derived SIT due to the different satellites and retrieval methods.

Some studies have been conducted to compare the differences between the various satellite-based SIT products. Wang et al. [26] compared the satellite products of CryoSat-2 from AWI and SMOS from University of Hamburg during 2011–2013, and found that the SIT of SMOS was 0.23 m smaller than the SIT of CryoSat-2 over the region where SIT is less than 1 m. Li et al. [27] focused on the comparison of different CryoSat-2 SIT products derived from AWI, National Snow and Ice Data Center (NSIDC), and European Space Agency (ESA), with the largest mean SIT in ESA and the smallest mean SIT in AWI during October–April from 2010 to 2018. Compared with OIB data, NSIDC shows the smallest bias and ESA exhibits the largest bias. Sallila et al. [28] evaluated the CryoSat-2 satellite products from various institutions and the CS2SMOS product over the period 2010–2017 based on the measurements obtained from the ULS observations of ice draft and the SIT data of OIB. The AWI CryoSat-2 and CS2SMOS datasets have the most robust ice draft with ULS observations, and the Jet Propulsion Laboratory (JPL) CryoSat-2 product shows the highest correlation with the SIT of OIB.

These mentioned studies primarily focus on the comparison and assessment between two different satellites. The comparison and evaluation of multi-source satellite-derived products are few, especially incorporating the satellite product from ICESat-2, which was launched in 2018, into the studies. This results in the limited comparison and evaluation of satellite SIT data in recent years. The types of observations used as the evaluation reference are also relatively homogeneous. The direct evaluation of SIT is mainly based on the OIB data. Since the ULS data only provides ice draft data, the direct evaluation of SIT based on this data is not straightforward. In addition, there is an important note that the latest versions of SIT products for CS2SMOS, CryoSat-2, and ICESat-2 had been released in October, November, and December 2023, respectively. The preceding research efforts were conducted based on the earlier data versions. It is believed that the latest versions of these satellite products have made improvements in the processing and retrieval of SIT. However, the detailed extent of distinctions among the latest versions of satellite products and their alignment with other observational data are still uncertain, requiring further investigations for conclusive findings.

Therefore, this study focused on the latest versions of SIT products and integrated the intercomparison and evaluation of various satellite data. Since SMOS has large uncertainties over the thick ice region [29], considering the overlap of time periods and coverage areas among multi-source satellite data, we selected the satellite data of ICESat-2, CryoSat-2, and CS2SMOS from October to April over the period 2018–2022 as the comparative objects. Furthermore, we evaluated the satellite-derived SIT products based on three types of evaluation data. In addition to the OIB data, two other kinds of SIT data were calculated from total thickness (SIT + snow depth) and retrieved from the ice draft, respectively. The

intercomparison and evaluation of diverse satellite-derived Arctic SIT products can provide a valuable insight and deeper understanding of the differences and reliabilities among the latest versions of SIT retrieval.

2. Data and Method

2.1. Satellite-Derived SIT Products

2.1.1. ICESat-2

The ICESat-2 was launched by National Aeronautics and Space Administration (NASA) in October 2018 [25]. The total freeboard measured by the ICESat-2 is the sum of sea ice freeboard and snow depth. The SIT is retrieved from the total freeboard data using the hydrostatic equilibrium based on a freeboard-to-thickness conversion. We used the latest version 3 of L4 monthly gridded SIT product with the spatial resolution of 25 km (Table 1). The ICESat-2 covers the sea ice growth season from October to April. The period of data used in this study is from November 2018 to April 2022.

Table 1. Introduction of the satellite and evaluation data used in this study.

Data Sets	Frequency	Temporal Range	Geographical Coverage	Grid Resolution	Data Sources
ICESat-2	Monthly	2018.11–2022.04	31.1°N–89.8°N	25 km	Petty et al. [30]
CryoSat-2	Monthly	2018.10–2022.04	16.6°N–89.8°N	25 km	Hendricks and Paul [31]
CS2SMOS	Weekly	2018.10–2022.04	16.6°N–89.8°N	25 km	Ricker et al. [24]
OIB	/	2019.04	Central Arctic and Greenland Sea	40 m	Kurtz et al. [32]
IceBird	/	2019.04	Central Arctic and Beaufort Sea	6–40 m	Jutila et al. [33]
ULS	Two-second	2018.10–2021.04	Beaufort Sea	/	Krishfield and Proshutinsky [34]

2.1.2. CryoSat-2

The CryoSat-2 satellite was launched by ESA in 2010 [35]. In this study, we selected the latest version 2.6 of L3 monthly CryoSat-2 SIT data derived from AWI in order to ensure the consistency of institution with CS2SMOS. The CryoSat-2 also covers the sea ice growth season from October to April. The spatial resolution of CryoSat-2 is 25 km and the period used is from October 2018 to April 2022 (Table 1).

2.1.3. CS2SMOS

The CryoSat-2 SIT product is based on measurements of the height of the ice surface above sea level, which has relatively large uncertainties in regions of thin ice, and the SMOS SIT product is based on surface brightness temperature (TB) evaluation, which has relatively small uncertainties over thin ice. Thus, the weekly CS2SMOS SIT data was developed by merging the two types of satellite data [24]. The latest version 206 of CS2SMOS used in this study maintains the same resolution and period with CryoSat-2 (Table 1).

2.2. Evaluation Data

2.2.1. OIB

NASA's OIB bridges the gap between the ICESat missions. It can provide high-resolution SIT data retrieved by the sea ice freeboard and snow depth data based on the hydrostatic equilibrium equation (Table 1). This study used the Quick Look version data provided by NSIDC since there is no overlap between other versions of OIB and the study period [16]. The Quick Look version data within the study period is only in April 2019. The tracks of OIB are mainly in the region of Central Arctic and Greenland Sea (Figure 1).

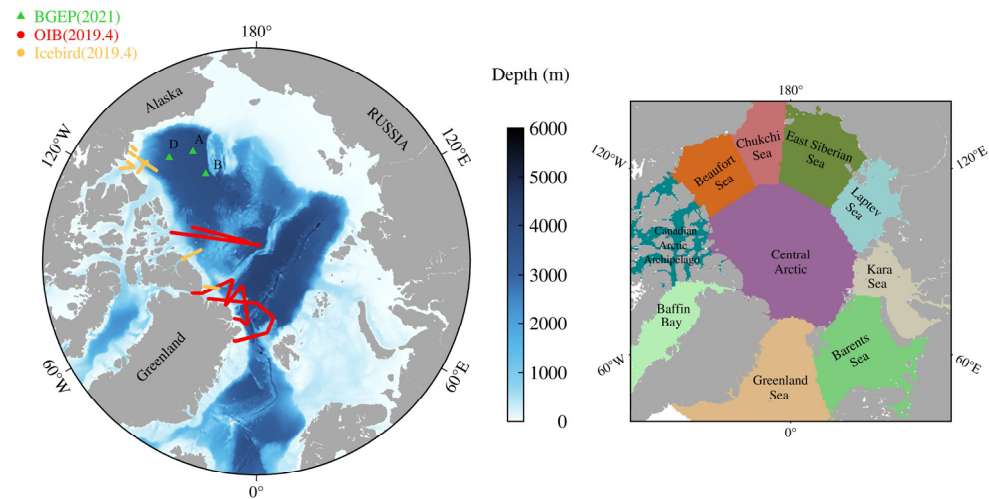


Figure 1. The geographic distribution of the evaluation data used in this study and the division of the Arctic Ocean region. The positions of the moorings A, B, and D associated with the BGEp are labeled.

2.2.2. AWI IceBird

The AWI's IceBird multi-sensor campaigns provide high-resolution total thickness and snow depth data [36]. To obtain the SIT data, the snow depth is subtracted from the total thickness. The SIT data within the study period is in April 2019 (Table 1). The tracks of AWI IceBird are mainly in the region of Central Arctic and Beaufort Sea (Figure 1).

2.2.3. Beaufort Gyre Exploration Project

Since 2003, the moorings with ULS instruments from Beaufort Gyre Exploration Project (BGEp) have provided continuous monitoring of ice draft (Figure 1). The ice draft data of BGEp has a complete 2 s time series and covers the study period from October 2018 to April 2021 [34]. The SIT can be retrieved from the ice draft. Since the ice draft has an estimation error of ± 0.05 – 0.1 m, the individual ULS draft measurement less than 0.1 m is excluded from the retrieval [28].

The equation of SIT retrieval can be expressed as:

$$h_i = \frac{\rho_w h_d - \rho_s h_s}{\rho_i} \quad (1)$$

where h_i is SIT, ρ_w is water density, h_d is ice draft, ρ_s is snow density, h_s is snow depth, and ρ_i is sea ice density. In this study, ρ_w is 1024 kg/m^3 , h_d is from BGEp, ρ_s from October to April is followed the method of Mallett et al. [3] and parameterized as:

$$\rho_s = 6.50t + 274.51 \quad (2)$$

where t is the number of months from 0 to 6 which represents the month from October to April, respectively. h_s is obtained from the Lagrangian snow-evolution model (SnowModel-LG) [37]. The version used in this study utilizes ERA5 atmospheric reanalysis data as its input. It is available from NSIDC and provides daily mean snow depth data with a spatial resolution of $25 \text{ km} \times 25 \text{ km}$. ρ_i is $916.7 \pm 35.7 \text{ kg/m}^3$ for first-year ice (FYI) and $882 \pm 23 \text{ kg/m}^3$ for multi-year ice (MYI), which is the most commonly used in algorithms for the retrieval of SIT, as proposed by Alexandrov et al. [38]. The distinction between MYI and FYI is based on the ice type of the CryoSat-2 product.

2.3. Sensitivity Cases of SIT Retrieval

According to Equation (1) above, the SIT retrieval from BGEp ice draft depends on the two key parameters: snow depth and sea ice density. In order to explore the impact of parameter schemes on the SIT retrieval and evaluation result of satellite products, we set

up five sensitivity cases. In each case, the water density, ice draft, and snow density are consistent with those used in the original SIT retrieval.

In the sensitivity cases, one additional scheme of snow depth and two additional schemes of sea ice density are included. For snow depth, due to the difference between the laser altimeter of the ICESat-2 and the radar altimeter of the CryoSat-2, Kwok et al. [39] used the freeboard differences from ICESat-2 and CryoSat-2 (IS2/CS2) to estimate snow depths. We used a monthly product of IS2/CS2 snow depth developed by Kacimi and Kwok [40] and the data period used is from October 2018 to April 2021. For sea ice density, Jutila et al. [36] obtained updated sea ice densities of $925.4 \pm 17.7 \text{ kg/m}^3$ for FYI and $902.4 \pm 19.4 \text{ kg/m}^3$ for MYI based on airborne measurements in 2019. In addition, the sea ice density of 915 kg/m^3 was used to estimate SIT in some studies [41–44].

Keeping the original snow depth data of SnowModel-LG (SMLG), we set up Case 1 and Case 2 by using two additional schemes of sea ice density. Then, replacing snow depth data by IS2/CS2, we set up Case 3–Case 5 by using the original and two additional schemes of sea ice density.

2.4. Satellite Products Intercomparisons

The intercomparison period is focused on four sea ice growth seasons (October–April) from 2018 to 2022. Due to the differences in spatiotemporal resolution, the study region is selected to be 65°N – 88°N . All SIT products have been interpolated to the generated grids with the resolution of $12.5 \times 12.5 \text{ km}$ by the inverse distance weighting (IDW) interpolation method in order to compare different satellite data products well. In particular, the weekly SIT data from CS2SMOS has been processed to monthly data, which is consistent with ICESat-2 and CryoSat-2 before interpolation.

In order to quantify the intercomparisons of three satellite products in detail, we used the pairwise comparison approach, which includes the comparisons between CryoSat-2 and ICESat-2, CS2SMOS and ICESat-2, and CS2SMOS and CryoSat-2. The metrics of difference, mean difference (MD), root mean squared error (RMSE), and correlation coefficient (CC) were used in the intercomparisons. In addition, the Arctic is divided into ten regions to focus on the regional pairwise comparison (Figure 1).

2.5. Satellite Products Evaluations

For the evaluation data of OIB, due to the high resolution of 40 m, the data grids are created along the trajectories at a 12.5 km interval. The SIT value of OIB over each data grid is calculated by averaging the OIB data within a 12.5 km range along the trajectory. The satellite data are interpolated to these data grids by IDW interpolation method.

Although the IceBird also has high-resolution data, the resolution varies from 6 to 40 m. Thus, we selected the same generated grids with 12.5 km and the SIT value of IceBird over each generated grid is calculated by averaging the IceBird data within a 12.5 km radius of each generated grid.

Since the sea ice drifting past the top of the mooring is measured by the ULS, the retrieved monthly mean SIT of each mooring from BGEP represents the regional mean SIT. We followed the method of Laxon et al. [22] to calculate the SIT over each mooring location by averaging the satellite data within 200 km radius of each mooring.

The metrics of MD, RMSE, CC, and Distance between Indices of Simulation and Observation (DISO) were used in the evaluations. DISO builds on the Euclidean Distance by providing a flexible approach to determining statistical metrics and their numbers [45]. A lower DISO value indicates a better ranking. In this study, we set up a synthetic metric that combines two statistical metrics of RMSE and CC to evaluate the performance of satellite products. The equation of DISO is defined as:

$$DISO_i = \sqrt{NRMSE_i^2 + (NCC_i - 1)^2} \quad (3)$$

where $i = 0, 1, \dots, m$, 0 indicates the observed data, and m is the total number of satellite products. $NRMSE$ and NCC represents the normalized metrics of RMSE and CC, respectively. The metrics are normalized to be between 0 and 1 and the normalization formula is expressed as:

$$NS_i = \frac{S_i - \min(S)}{\max(S) - \min(S)} \quad (4)$$

where S indicates the metric, such as RMSE and CC. When $i = 0$, the metrics of RMSE and CC between the observed data and itself are 0 and 1, respectively.

3. Results

3.1. Intercomparisons of Satellite Products

3.1.1. Spatiotemporal SIT Differences of Three Satellite Products

In general, the three satellite products showed the similar major distribution patterns of SIT, but had noticeable differences in values (Figure 2). All three products captured the larger SIT north of the Canadian Arctic Archipelago (CAA) and Greenland, and smaller SIT in the Barents and Kara Seas and along the Northeast Greenland shelf. In addition, the relatively low values in the Baffin Bay were found by both CryoSat-2 and CS2SMOS. The spatial mean SIT of ICESat-2, CryoSat-2 and CS2SMOS was 1.22 m, 1.15 m, and 1.04 m, respectively.

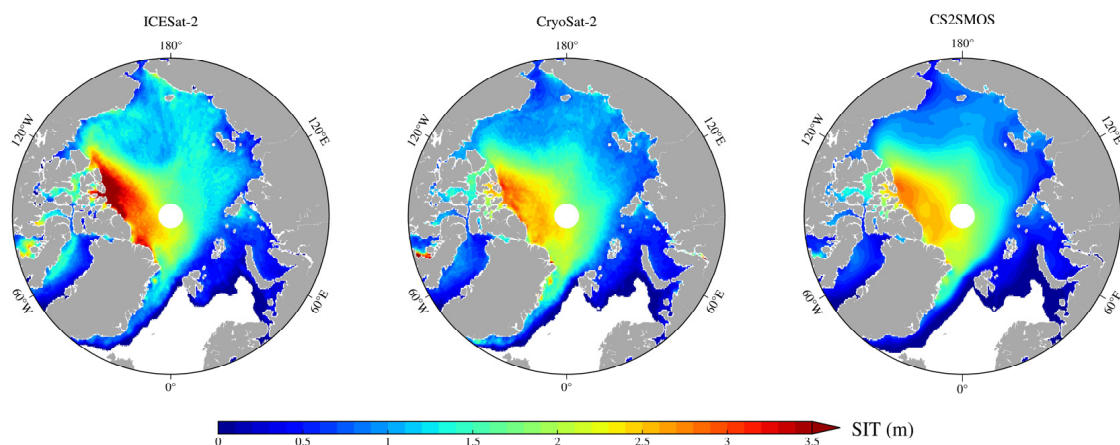


Figure 2. Spatial distribution of multi-year mean SIT for ICESat-2, CryoSat-2 and CS2SMOS over the period 2018–2022.

The monthly variations of spatial mean SIT over the period 2018–2022 were highly correlated ($CC > 0.9$, $p < 0.01$) among the three satellite products (Figure 3). However, due to the differences in SIT values, they showed different freezing months. The CryoSat-2 data indicated that the freezing month was October, while the ICESat-2 data indicated that the freezing month was November. The CS2SMOS data showed November as the freezing month during 2019–2020 and October as the freezing month in 2018 and 2021. In terms of the SIT differences between melting month (April) and freezing month (October or November) each year, CryoSat-2 had the largest differences with the maximum value of 0.82 m in 2019, while CS2SMOS had the smallest, with the minimum value of 0.57 m in 2021.

3.1.2. Pairwise Comparison of Satellite Products

To compare the spatiotemporal differences of SIT from the three satellite products in detail, the pairwise comparison was conducted by categorizing the three products into three groups, each containing two satellite datasets.

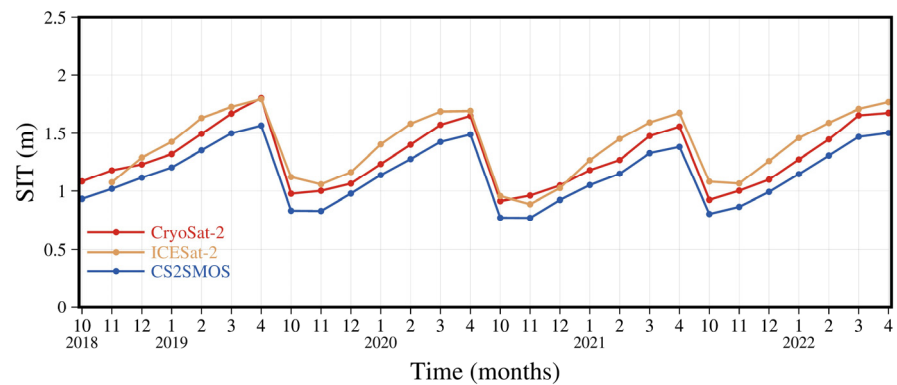


Figure 3. Monthly variations of spatial mean SIT from ICESat-2, CryoSat-2 and CS2SMOS over the period 2018–2022.

In group 1 of CryoSat-2 and ICESat-2, the difference is defined as the result of CryoSat-2 minus ICESat-2. The spatial distribution of multi-year monthly mean SIT suggested that the Arctic primarily manifested negative differences throughout most months, with positive differences observed only in October and November, generally indicating the larger SIT in ICESat-2 (Figure 4). The positive differences were concentrated in the Central Arctic. As the SIT increases, the area of positive differences gradually extended to the Kara Sea, Barents Sea, Greenland Sea, and Baffin Bay, and in particular, in the marginal ice zone (MIZ) of Barents Sea and Greenland Sea. The negative differences usually occurred north of the CAA and Greenland, indicating that CryoSat-2 generally had smaller SIT than ICESat-2. From December to April, the negative areas were concentrated in the Beaufort Sea, Chukchi Sea, East Siberian Sea, and Laptev Sea. In months characterized by negative differences, January records the highest percentage at 66%, while the MD reaches its maximum in February at -0.16 m (Figure 5). The RMSE of SIT between CryoSat-2 and ICESat-2 was the smallest in December. Further analyses of seasonal mean SIT in the different regions based on CC and RMSE exhibited that the two satellite products matched better in the Beaufort Sea and Central Arctic for three seasons (Figure 6). In these two regions, CryoSat-2 and ICESat-2 in winter (December–February) have the higher correlation ($CC > 0.9$, $p < 0.01$). In the other regions except the CAA, the overall correlation between the two products is relatively weak during the fall, marked by larger RMSE. In general, there are relatively large differences of SIT with larger RMSE and lower CC in the Barents Sea between CryoSat-2 and ICESat-2.

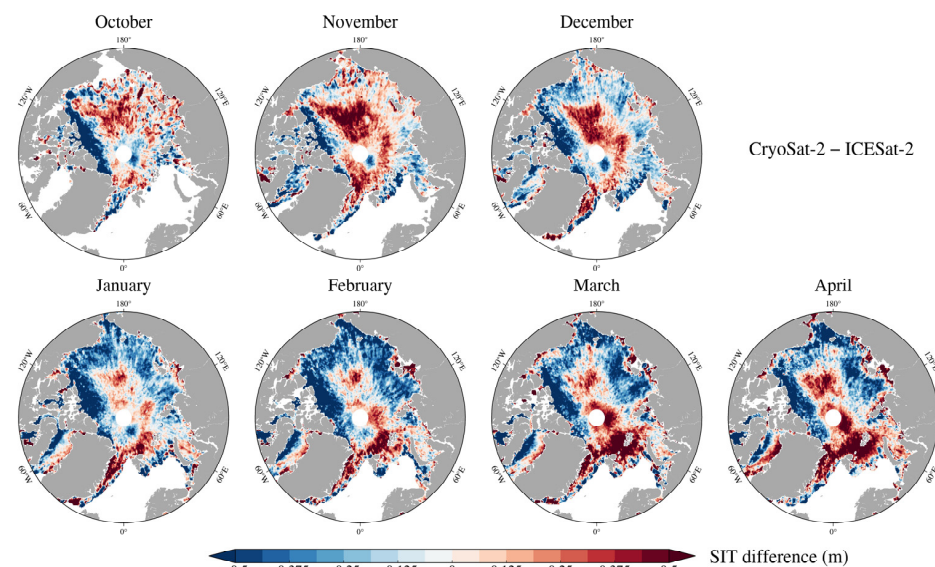


Figure 4. Spatial distribution of multi-year monthly mean SIT differences between CryoSat-2 and ICESat-2 over the period 2018–2022.

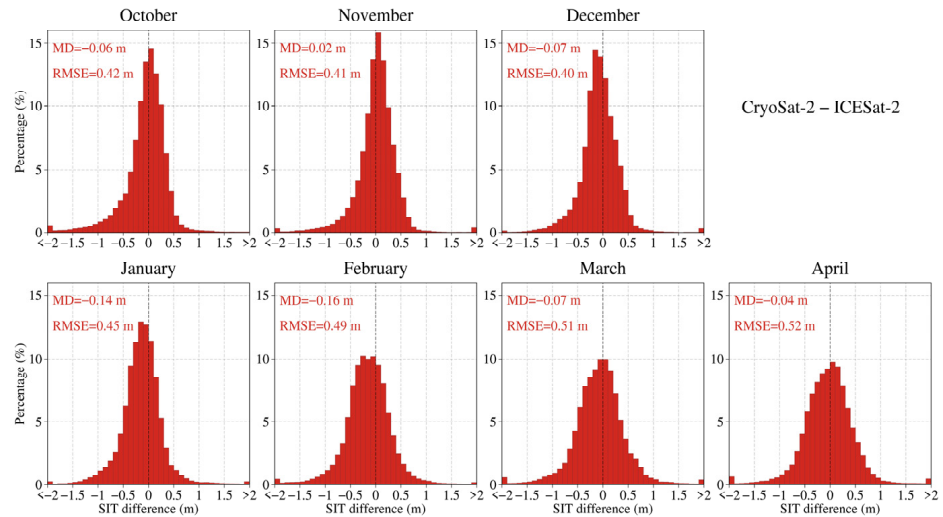


Figure 5. Histogram of multi-year monthly mean SIT differences between CryoSat-2 and ICESat-2 over the period 2018–2022.

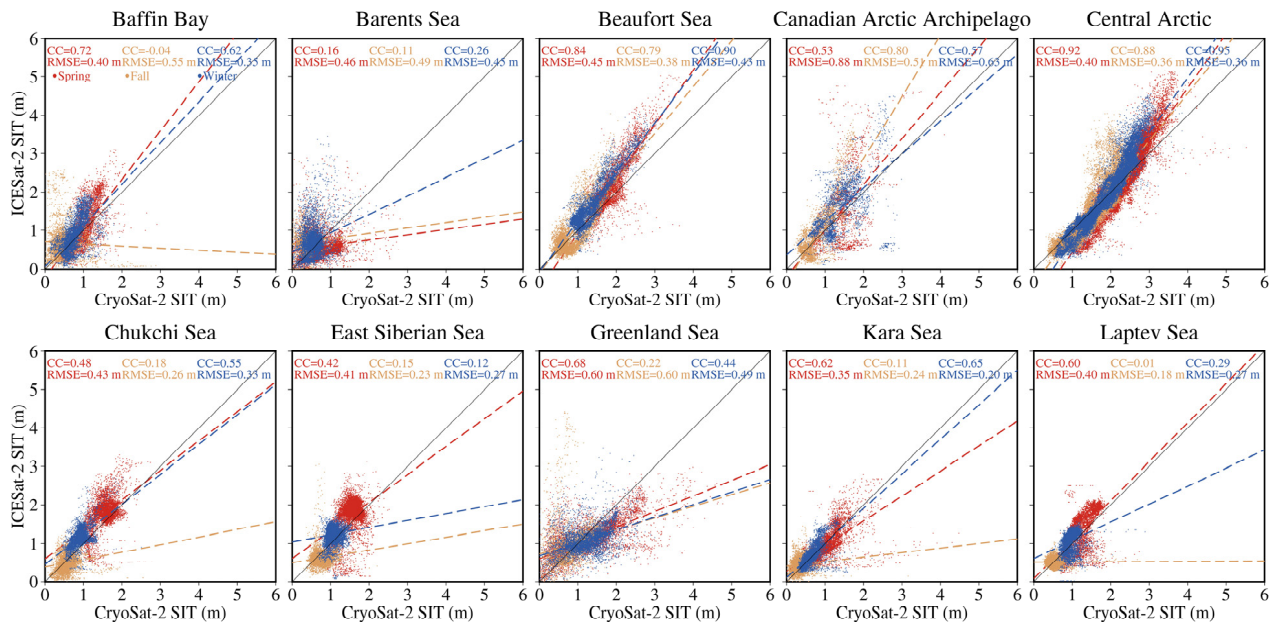


Figure 6. Comparison of seasonal mean SIT between CryoSat-2 and ICESat-2 in the different regions. The solid black line depicted signifies the optimal fitting line.

In group 2 of CS2SMOS and ICESat-2, the difference is defined as the result of CS2SMOS minus ICESat-2. Based on the pairwise comparisons of group 1 and group 2, it is clear that ICESat-2 generally showed the largest mean SIT. The spatial distribution of multi-year monthly mean SIT differences showed that the negative differences dominated in the Arctic, indicating the smaller SIT in CS2SMOS (Figure 7). There were no significant differences in the distribution pattern of differences during the different months. The negative differences dominated in most regions. In particular, in the north of the CAA and Greenland, the negative differences mean that CS2SMOS also had smaller SIT than ICESat-2. The positive differences were mainly in the Central Arctic. As the SIT increases, some areas of positive differences gradually extended to the Northeast Greenland shelf, Barents Sea, and Kara Sea. However, the area of the positive differences in these three regions was much smaller than the area between CryoSat-2 and ICESat-2. The percentage of negative differences between CS2SMOS and ICESat-2 was larger than 65% in each month with a maximum value of 77% in January, and the MD had the largest negative value of

−0.27 m in February (Figure 8). The RMSE between CS2SMOS and ICESat-2 was similar to the RMSE between CryoSat-2 and ICESat-2 in each month. Additionally, the MD consistently exceeded that of the MD between CryoSat-2 and ICESat-2 in each corresponding month, suggesting that ICESat-2 had the closer SIT with CryoSat-2 than with CS2SMOS. Similar to group 1, the seasonal mean pairwise comparison in group 2 between CS2SMOS and ICESat-2 also exhibited better match in the Beaufort Sea and Central Arctic for three seasons, with higher CC values during winter and lower RMSE in the fall (Figure 9). Except for the CAA, the comprehensive correlation between the two products also showed relative weakness during the fall, characterized by higher RMSE. The relatively large differences are mainly in the East Siberian Sea and Barents Sea.

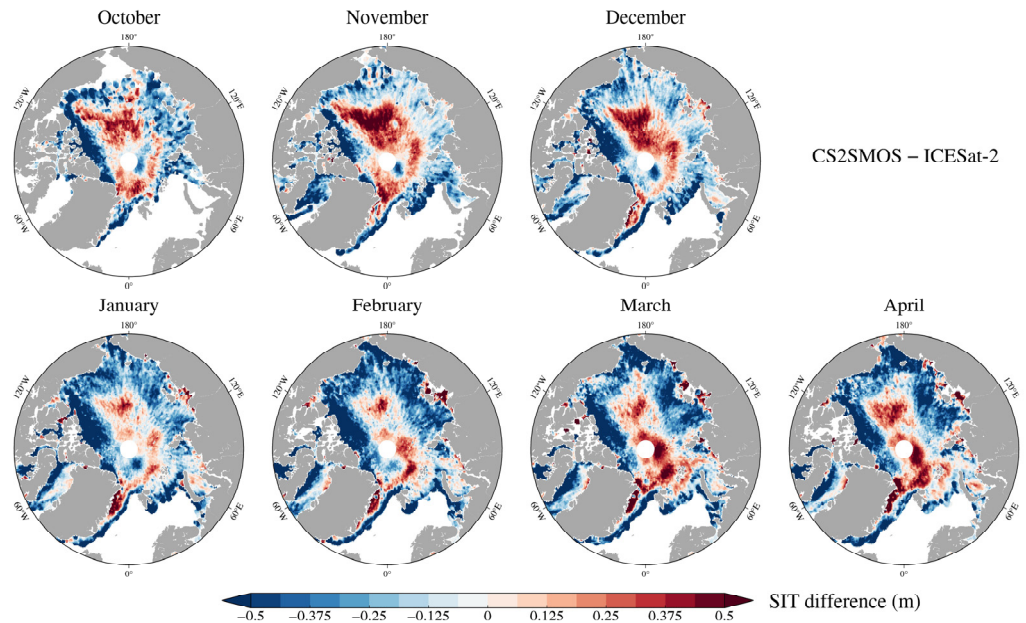


Figure 7. Spatial distribution of multi-year monthly mean SIT differences between CS2SMOS and ICESat-2 over the period 2018–2022.

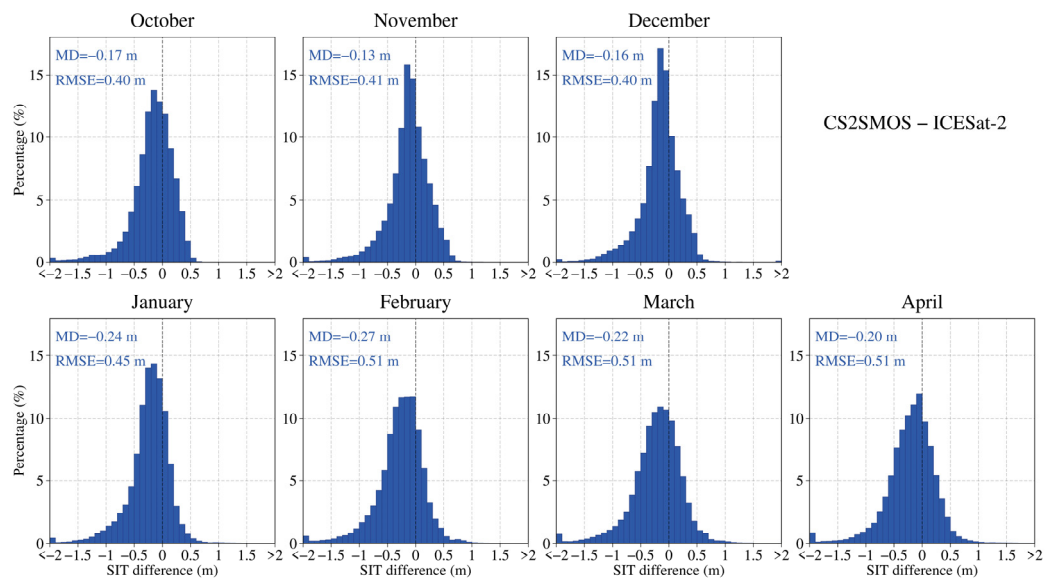


Figure 8. Histogram of mean SIT differences between CS2SMOS and ICESat-2 over the period 2018–2022.

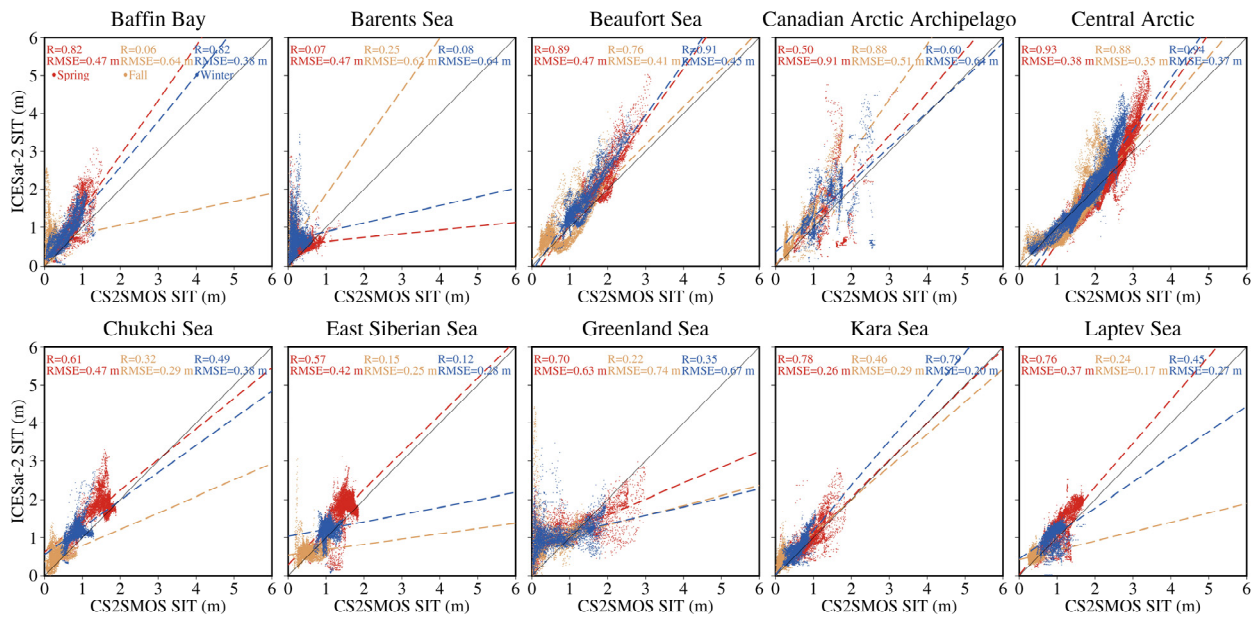


Figure 9. Comparison of seasonal mean SIT between CS2SMOS and ICESat-2 in the different regions. The solid black line depicted signifies the optimal fitting line.

In group 3 of CS2SMOS and CryoSat-2, the difference is defined as the result of CS2SMOS minus CryoSat-2. Based on the pairwise comparisons from group 1 to group 3, it is clear that CS2SMOS showed the smallest results. Therefore, it is not surprising that the spatial distribution of multi-year monthly mean SIT differences in group 3 revealed a dominance of negative differences in the Arctic, especially in the regions of thin ice, such as MIZ (Figure 10). Correspondingly, the percentage of negative differences between CS2SMOS and CryoSat-2 was dominant in all the months with the largest negative MD of -0.18 m in April (Figure 11). The pairwise comparison of seasonal SIT in group 3 also exhibited a better match in the Beaufort Sea and Central Arctic for three seasons (Figure 12). The relatively large differences are mainly in the Kara Sea and Barents Sea.

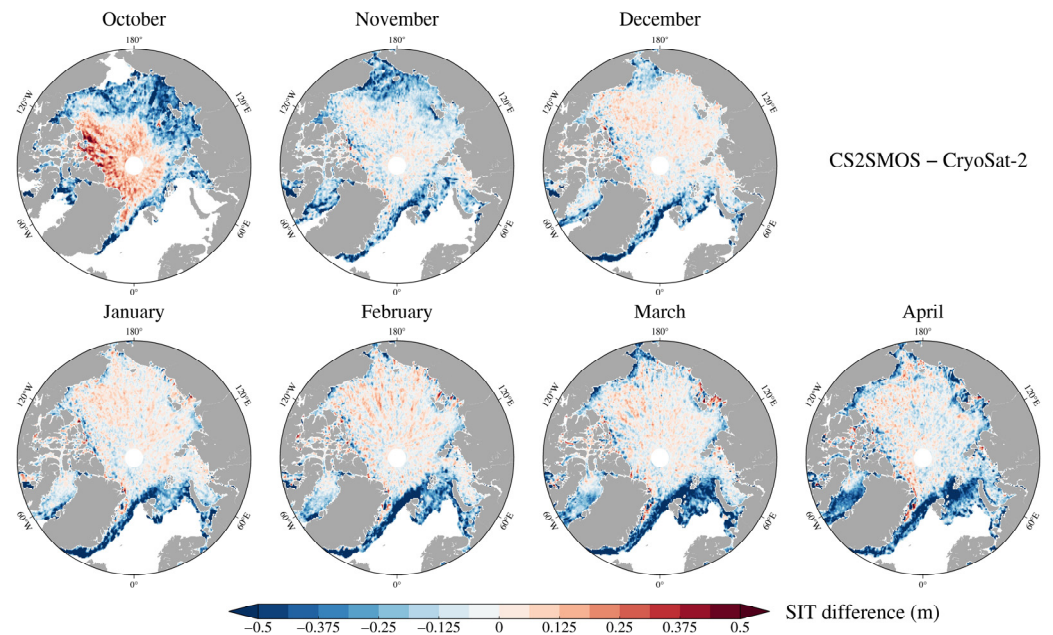


Figure 10. Spatial distribution of multi-year monthly mean SIT differences between CS2SMOS and CryoSat-2 over the period 2018–2022.

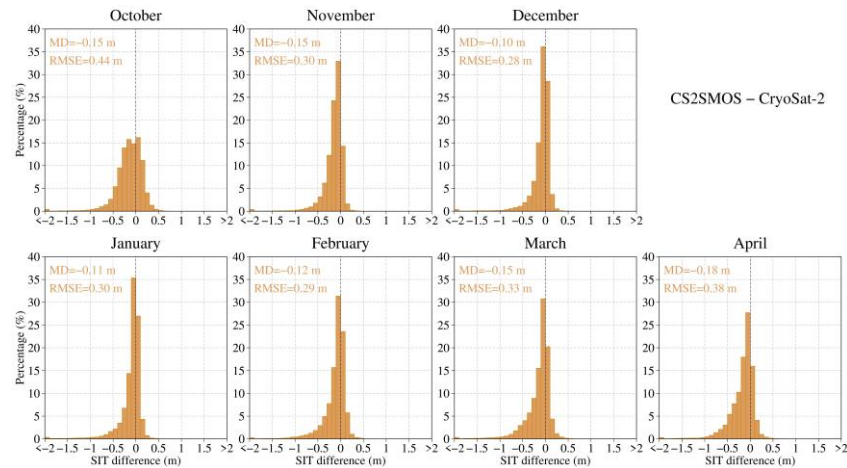


Figure 11. Histogram of mean SIT differences between CS2SMOS and CryoSat-2 over the period 2018–2022.

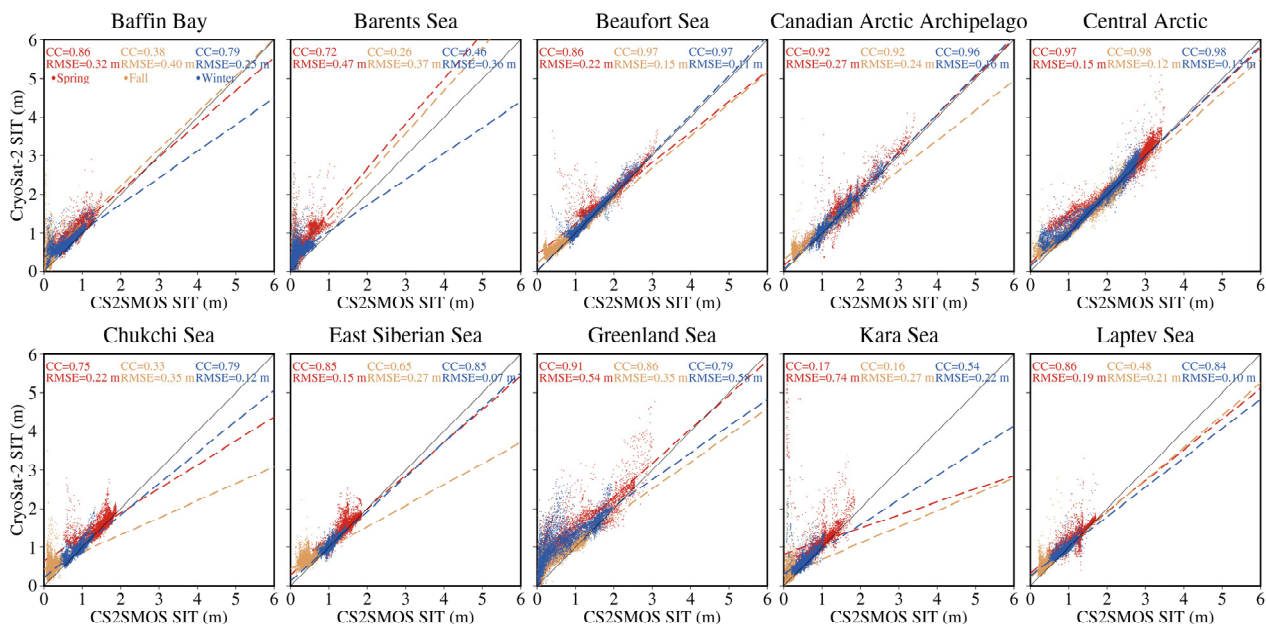


Figure 12. Comparison of seasonal mean SIT between CS2SMOS and CryoSat-2 in the different regions. The solid black line depicted signifies the optimal fitting line.

3.2. Evaluations of Satellite Products

The preceding comparative analysis of the three satellite-derived SIT only allows the quantification of the extent of differences among diverse satellite data. Nevertheless, for the evaluation of errors in satellite SIT, it is imperative to depend on comparisons with the airborne and in situ observational data.

During the study period 2018–2022, the only available OIB data is in April 2019. There are four airborne campaigns were used in this month. Note that, since the campaigns take a relatively short time, the SIT data along the flight track only represent spatial variations. In order to evaluate the spatial variations of different satellite products, the sections are defined along the trajectories of OIB data (Figure 13). In general, all products demonstrated an underestimation of OIB, with ICESat-2 displaying higher values for both RMSE. Taking into account the two metrics of varying RMSE and CC comprehensively, the DISO revealed that CS2SMOS had the best match with the OIB data, as evidenced by the highest CC values in two campaigns and the lowest RMSE values in all campaigns (Table 2).

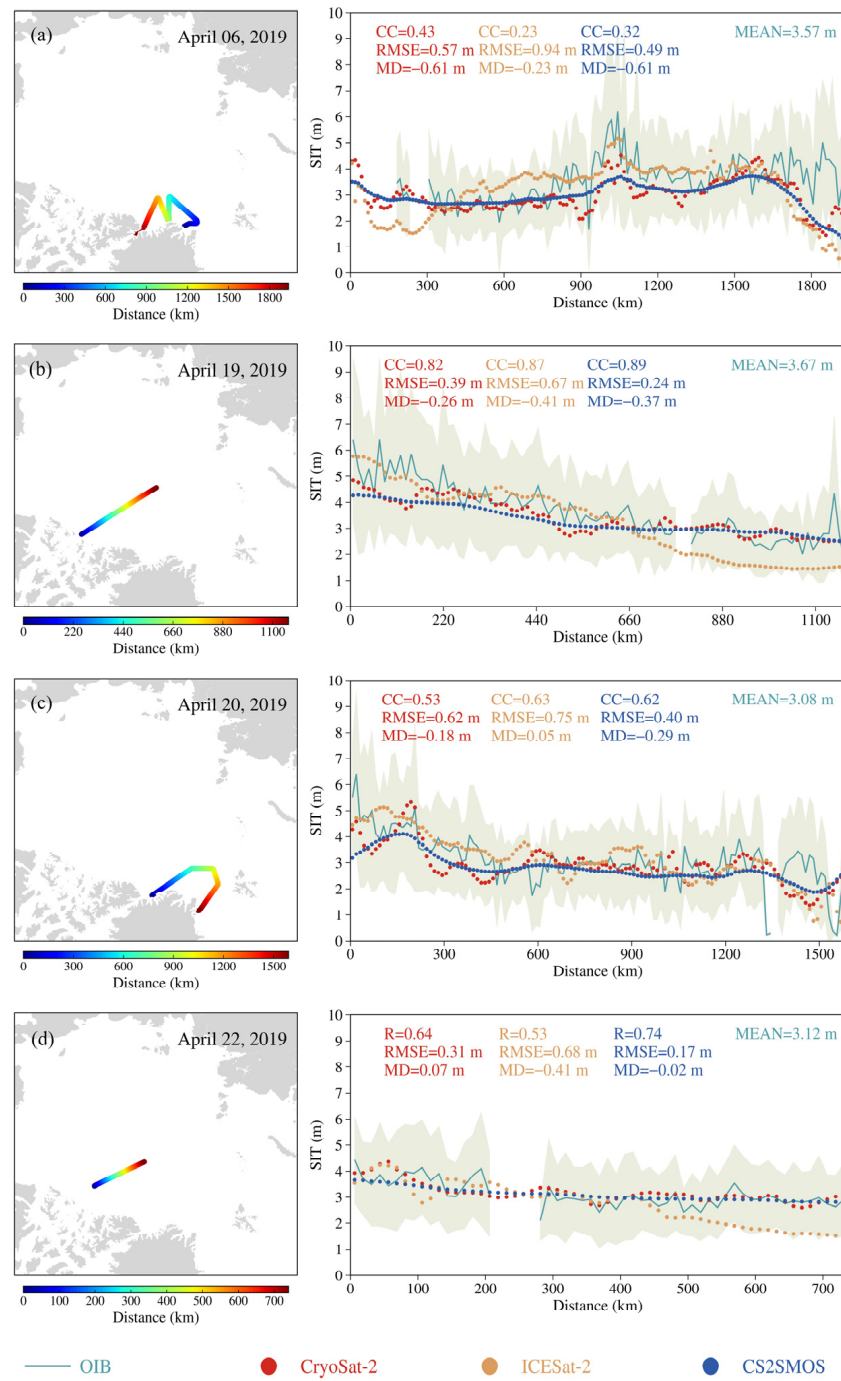


Figure 13. Evaluation of satellite-derived SIT along the OIB trajectory in the campaigns of (a) 6 April 2019, (b) 19 April 2019, (c) 20 April 2019, and (d) 22 April 2019. The OIB trajectory is shown in the left panel, with the colors representing the distance from the starting position. The variation of SIT along the trajectory for the OIB and the satellite products are shown in the right panel. Shading indicates the standard deviation of OIB SIT.

Table 2. DISO values of satellite products with airborne and in situ observations.

	CryoSat-2	ICESat-2	CS2SMOS
OIB	1.333 (CC: 0.58, RMSE: 0.82)	1.389 (CC: 0.59, RMSE: 0.93)	1.276 (CC: 0.61, RMSE: 0.82)
IceBird	0.997 (CC: 0.80, RMSE: 0.75)	1.414 (CC: 0.75, RMSE: 1.26)	1.035 (CC: 0.79, RMSE: 0.78)
BGEP	1.414 (CC: 0.91, RMSE: 0.26)	1.184 (CC: 0.93, RMSE: 0.23)	1.180 (CC: 0.93, RMSE: 0.23)
All	1.072 (CC: 0.79, RMSE: 0.76)	1.414 (CC: 0.73, RMSE: 1.01)	1.070 (CC: 0.80, RMSE: 0.77)

The evaluation with the IceBird data is also in April 2019 and suggested that the mean SIT of all products were underestimated. Compared to ICESat-2, the scatter plots in CryoSat-2 and CS2SMOS had smaller dispersions (Figure 14). Among the three products, ICESat-2 showed the largest DISO with lowest CC and the largest RMSE, thus indicating the largest difference with the IceBird data (Table 2). The CryoSat-2 had the best performance with the IceBird data.

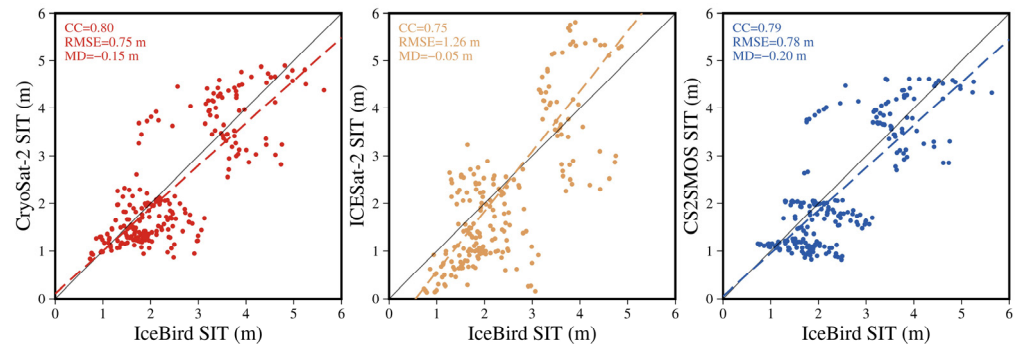


Figure 14. Evaluation of satellite-derived SIT with the IceBird data. The solid black line depicted signifies the optimal fitting line.

The evaluation results from the three moorings of BGEP revealed that all the three satellite products showed a reasonable agreement of time series variation with BGEP data during October 2018–April 2021 (Figure 15). The ICESat-2 had the smallest difference at mooring A and B, whereas the CS2SMOS had the smallest difference at mooring D, with the highest CC and the smallest RMSE. The DISO of all the three moorings revealed that the CS2SMOS had the best performance (Table 2).

Based on the comprehensive evaluation of OIB, IceBird, and BGEP, the CS2SMOS generally had the best match with the airborne and in situ observational data, and the CryoSat-2 performed better than ICESat-2 (Table 2).

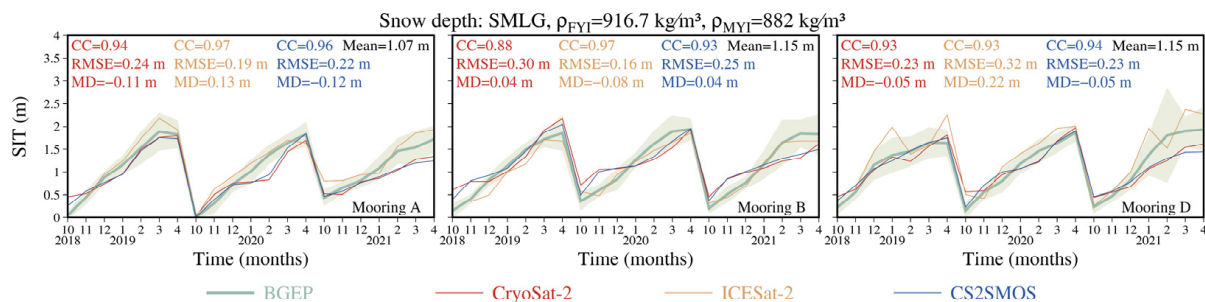


Figure 15. Time series evaluations of monthly satellite-derived SIT with the three moorings from BGEP. Shading indicates the standard deviation of monthly BGEP SIT.

4. Discussion

When employing a hydrostatic equilibrium equation for SIT estimation, the accuracy of the satellite-derived SIT depends on some important factors, such as snow depth, sea ice freeboard, and total freeboard, whether obtained by laser or radar altimetry. In addition, the impacts of density parameters on the SIT retrieval also cannot be ignored. In the evaluation with BGEP data, we used ice drafts to derive SIT-based on the hydrostatic equilibrium, which is affected by the choice of snow depth and sea ice density. In order to explore whether the evaluation results of the three satellite products based on retrieved SIT from BGEP are influenced by different snow depths and sea ice densities, the five sensitivity cases were conducted.

Overall, the changes of SIT retrieval in the five cases were very slight (Figure 16). The differences of mean SIT of BGEP between the original SIT retrieval and the five cases were

less than 0.02 m for the three moorings, causing the very similar metrics of CC and RMSE in all the cases. Therefore, the SIT retrieval of BGEP using the different snow depths and sea ice densities did not influence the performance ranking of the three satellite products and the original evaluation result was robust (Table 3).

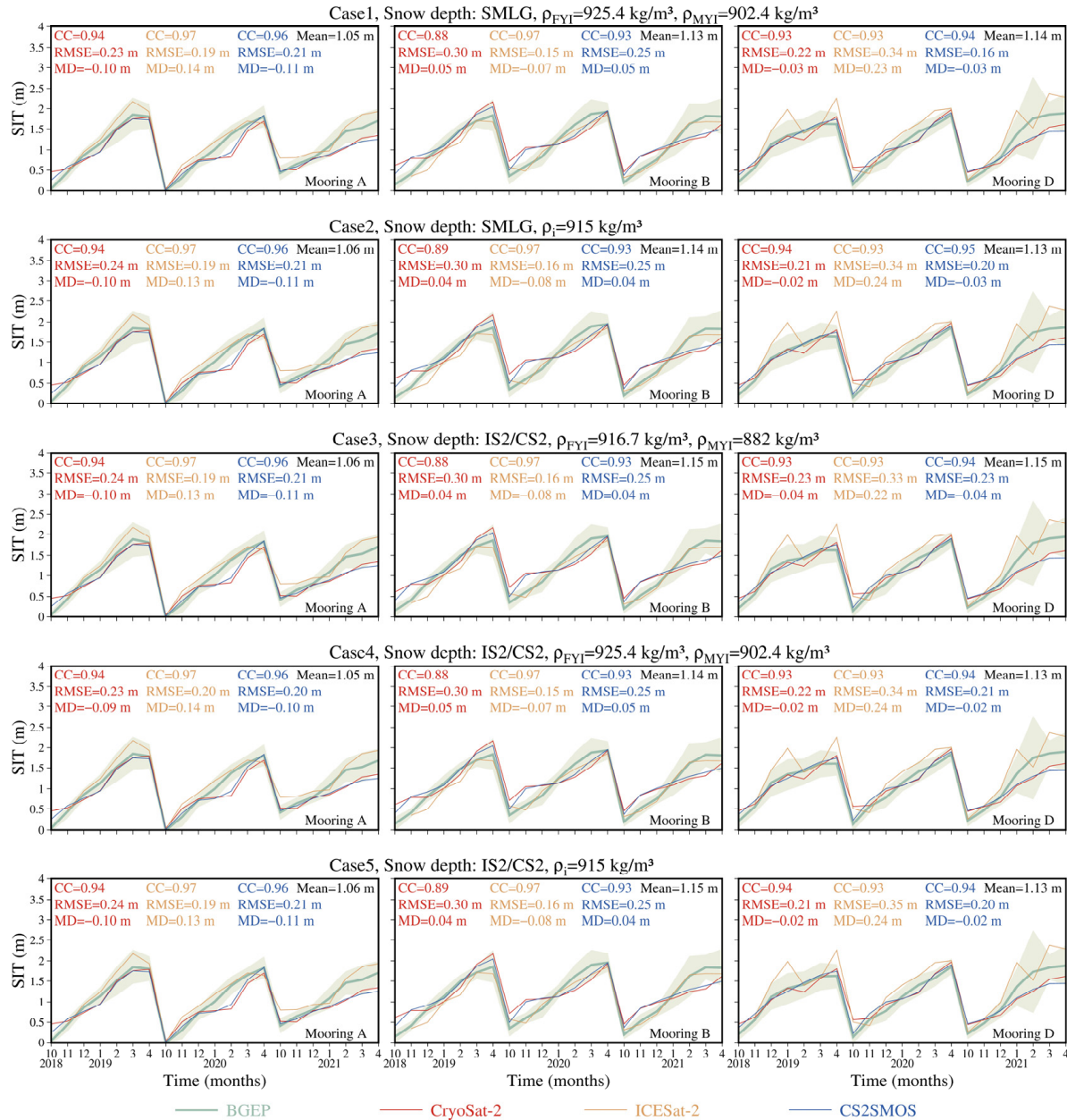


Figure 16. Time series evaluations of satellite-derived SIT with the five cases in the BGEP using different snow depth and sea ice density. Shading indicates the standard deviation of monthly BGEP SIT.

Table 3. DISO values of satellite products with the five cases in the BGEP using different snow depth and sea ice density.

	CryoSat-2	ICESat-2	CS2SMOS
BGEP Case1			
Snow depth: SMLG (0.001–0.288 m)			
$\rho_{FYI} = 925.4\text{kg/m}^3$,	1.414	0.894	0.823
$\rho_{MYI} = 902.4\text{kg/m}^3$			

Table 3. Cont.

	CryoSat-2	ICESat-2	CS2SMOS
BGEP Case2 Snow depth: SMLG (0.001–0.288 m) $\rho_i = 915\text{kg/m}^3$	1.414	0.908	0.812
BGEP Case3 Snow depth: IS2/CS2 (0.021–0.219 m) $\rho_{\text{FYI}} = 916.7\text{kg/m}^3$, $\rho_{\text{MYI}} = 882\text{kg/m}^3$	1.414	0.880	0.823
BGEP Case4 Snow depth: IS2/CS2 (0.021–0.219 m) $\rho_{\text{FYI}} = 925.4\text{kg/m}^3$, $\rho_{\text{MYI}} = 902.4\text{kg/m}^3$	1.414	0.899	0.820
BGEP Case5 Snow depth: IS2/CS2 (0.021–0.219 m) $\rho_i = 915\text{kg/m}^3$	1.414	0.913	0.811

A further analysis was focused on the spatiotemporal differences of SIT between FYI and MYI. The comparison results revealed that the variation pattern of SIT for FYI closely aligns with the overall pattern of Arctic sea ice. Generally, ICESat-2 displayed the largest SIT for FYI, followed by CryoSat-2 and CS2SMOS (Figure 17). This can be attributed to the dominant area coverage of FYI in most months from October to April. However, for MYI, CS2SMOS mostly exhibited larger SIT than CryoSat-2. In addition, the freezing month of three satellite products for FYI and MYI consistently indicated to be October except in 2020 for FYI of ICESat-2. Moreover, the evaluation of SIT between FYI and MYI with the reference data were also conducted. Since the majority of BGEP and OIB data were located in the regions of FYI and MYI, respectively, only the IceBird data can be utilized in this evaluation. The percentage of FYI and MYI data in IceBird was about 58.3% and 41.7%. The evaluation results indicated that both FYI and MYI from CryoSat-2 exhibited the best agreement with IceBird data (Table 4), which was consistent with the overall evaluation result with IceBird in Table 2.

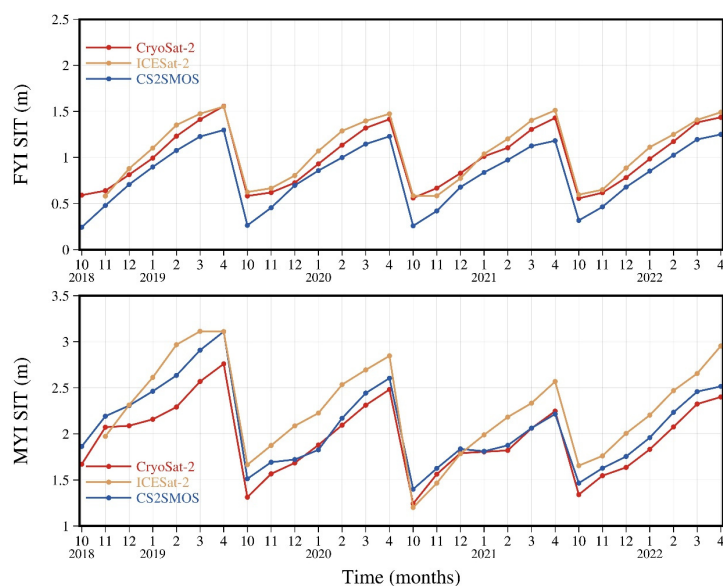


Figure 17. Monthly variations of spatial mean SIT of FYI and MYI from ICESat-2, CryoSat-2, and CS2SMOS over the period 2018–2022.

Table 4. DISO values of satellite products for FYI and MYI with IceBird data.

	ICESat-2	CryoSat-2	CS2SMOS
IceBird (FYI)	1.414	1.120	1.181
IceBird (MYI)	1.414	0.721	1.008

This study involves SIT products from three satellites of CryoSat-2, ICESat-2, and SMOS. The reasons for differences in SIT retrieval among these satellites are various, with primary factors including the measurement instruments, retrieval methods, and data parameters used. In terms of measurement instruments, CryoSat-2 utilizes a radar altimeter, ICESat-2 employs a laser altimeter, and SMOS relies on a microwave imaging radiometer. Regarding retrieval methods, both CryoSat-2 and ICESat-2 utilize the hydrostatic equilibrium equation to derive SIT from sea ice freeboard. However, the two satellites employ different approaches to obtain the sea ice freeboard. CryoSat-2 transforms the radar freeboard into the sea ice freeboard through radar signal speed correction, while ICESat-2 estimates the sea ice freeboard by subtracting snow depth data from measured total freeboard. SMOS uses a three-layer dielectric slab model to derive SIT-based on measured brightness temperature. In terms of data parameters, CryoSat-2 and ICESat-2 utilize different snow depth datasets. CryoSat-2 uses a combined snow depth data from climatology and passive microwave remote sensing, while ICESat-2 applies snow depth data from the NASA Eulerian Snow On Sea Ice Model (NESOSIM). In addition, the scheme of sea ice and snow densities between CryoSat-2 and ICESat-2 are also different. CryoSat-2 defines sea ice density as 917 kg/m^3 for first-year ice and 882 kg/m^3 for multi-year ice, while ICESat-2 selects a consistent density of 915 kg/m^3 for both ice types. The snow densities are parameterized based on Equation (2) in this study for CryoSat-2 and obtained from NESOSIM for ICESat-2, respectively. Notably, it has been documented that snow grain size and snow salinity profiles can potentially cause errors in SIT retrieval. The increase in snow grain size can lead to an overestimation of snow depth when measured using satellite microwave radiometry. Consequently, the uncertainty in the snow depth parameter, used for SIT retrieval, further contributes to potential errors in satellite-based SIT estimates [46]. Moreover, Nandan et al. [47] demonstrated that snow salinity on FYI significantly affects the accuracy of SIT estimations, attributable to snow salinity profiles causing the main radar scattering interface to shift relative to the snow-ice interface.

5. Conclusions

Since the launch of ICESat-2 satellite in 2018, the quantitative intercomparisons and evaluations of SIT data from multiple satellite sources in recent years are few. This study specifically compared the spatiotemporal differences in SIT products obtained from the ICESat-2, CryoSat-2, and CS2SMOS satellites during the period from October to April in 2018–2022. Furthermore, the evaluations of the three satellite products were conducted based on some observational data with the overlapping time periods including the airborne data from OIB and IceBird, and the in situ data from BGEP.

Generally, the three satellite products displayed similarly primary distribution patterns of SIT, but had noticeable differences of derived SIT values. From the perspective of the entire Arctic region, the mean SIT exhibited the characteristics of ICESat-2 data being the largest, followed by CryoSat-2 data, and CS2SMOS data being the smallest. The ICESat-2 product had the closer SIT with CryoSat-2 product than with CS2SMOS product. Although the monthly variations of spatial mean SIT over the period 2018–2022 were highly correlated among the three satellite products, there were differences of freezing month. The CryoSat-2 data suggested October as the freezing month, whereas the ICESat-2 data indicated November. For CS2SMOS, the freezing month was noted as November in 2019–2020 and October in 2018 and 2021.

The three satellite products suggested significant differences in various regions. In the region north of the CAA and Greenland, ICESat-2 data showed the largest SIT, while the SIT from CryoSat-2 and CS2SMOS data is similar. In the regions of thin ice, such as MIZ, CryoSat-2 data showed the maximum thickness, followed by ICESat-2, with CS2SMOS recording the smallest thickness. The three satellite products had the best agreements of SIT in the regions of Beaufort Sea and Central Arctic, in particular in winter, and had the most distinct differences in the Barents Sea.

The evaluation results revealed that CS2SMOS had the best match with OIB and BGEP data, and CryoSat-2 mated the best with IceBird data. Based on comprehensive evaluations, CS2SMOS had the best performance with the airborne and in situ observational data, and the CryoSat-2 had better performance than ICESat-2. Note that this evaluation result depends on the regions and time periods with available observational data. The further assessment of satellite-derived SIT are required with the support from more observational data.

The diverse temporal and spatial coverage provided by different satellites facilitates the observation of long-term trends and patterns, contributing to a more profound understanding of the impacts of climate change on the Arctic region. Additionally, the geographical distribution covered by various satellites ensures a broader perspective, enhancing our ability to monitor sea ice rapid change across a global scale. Overall, the intercomparisons and evaluations of the latest versions of satellite-derived Arctic SIT offers fresh insights and benefits for understanding the intricate dynamics and thermodynamics of Arctic sea ice.

Author Contributions: Conceptualization, Y.Z. (Yu Zhang) and C.C.; methodology, F.C., D.W. and Y.Z. (Yi Zhou); validation, F.C., D.W. and Y.Z. (Yu Zhang); formal analysis, F.C. and D.W.; data curation, F.C.; writing—original draft preparation, F.C., D.W. and Y.Z. (Yu Zhang); writing—review and editing, Y.Z. (Yi Zhou) and C.C.; visualization, F.C. and D.W. All authors have read and agreed to the published version of the manuscript.

Funding: This research was funded by the National Key Research and Development Program of China (No. 2019YFA0607001), the National Natural Science Foundation of China (No. 42376231 and No. 42130402), the Natural Science Foundation of Shanghai (No. 22ZR1427400), and the Innovation Group Project of Southern Marine Science and Engineering Guangdong Laboratory (Zhuhai) (No. 311022006).

Data Availability Statement: The sea ice thickness data of ICESat-2 is available at <https://nsidc.org/data/is2sitmogr4/versions/3>, accessed on 15 December 2023. The sea ice thickness data of CryoSat-2 is available at ftp://ftp.awi.de/sea_ice/product/cryosat2/v2p6/nh/l3c_grid/month, accessed on 11 December 2023. The CS2SMOS sea ice thickness product is obtained from ftp://ftp.awi.de/sea_ice/product/cryosat2_smos/v206, accessed on 10 December 2023. The Quick Look version of OIB data is collected from <https://nsidc.org/data/nsidc-0708/versions/1>, accessed on 16 December 2022. The AWI IceBird data is available at <https://doi.pangaea.de/10.1594/PANGAEA.933912>, accessed on 20 December 2022. The ice draft of ULS from BGEP is downloaded from <https://www2.whoi.edu/site/beaufortgyre/data/mooring-data>, accessed on 22 December 2022. The snow depth from SnowModel-LG is available at <https://nsidc.org/data/nsidc-0758/versions/1>, accessed on 26 December 2022. The IS2/CS2 snow depth data is obtained from <https://icesat-2.gsfc.nasa.gov/sea-ice-data/kacimi-kwok-2022>, accessed on 26 December 2022.

Acknowledgments: We would like to thank the editors and the anonymous reviewers for their constructive comments and advice.

Conflicts of Interest: The authors declare no conflicts of interest.

References

1. Budikova, D. Role of Arctic Sea Ice in Global Atmospheric Circulation: A Review. *Glob. Planet. Chang.* **2009**, *68*, 149–163. [[CrossRef](#)]
2. Guemas, V.; Blanchard-Wrigglesworth, E.; Chevallier, M.; Day, J.J.; Déqué, M.; Doblas-Reyes, F.J.; Fučkar, N.S.; Germe, A.; Hawkins, E.; Keeley, S.; et al. A Review on Arctic Sea-ice Predictability and Prediction on Seasonal to Decadal Time-scales. *Q. J. R. Meteorol. Soc.* **2016**, *142*, 546–561. [[CrossRef](#)]

3. Mallett, R.D.C.; Lawrence, I.R.; Stroeve, J.C.; Landy, J.C.; Tsamados, M. Brief Communication: Conventional Assumptions Involving the Speed of Radar Waves in Snow Introduce Systematic Underestimates to Sea Ice Thickness and Seasonal Growth Rate Estimates. *Cryosphere* **2020**, *14*, 251–260. [[CrossRef](#)]
4. Zhang, Y.; Chen, C.; Shen, X.; Xu, D.; Shao, W.; Beardsley, R.C.; Chang, L.; Feng, G. Role of Sea Level Pressure in Variations of the Canadian Arctic Archipelago Throughflow. *Adv. Clim. Chang. Res.* **2021**, *12*, 539–552. [[CrossRef](#)]
5. Carmack, E.C.; Yamamoto-Kawai, M.; Haine, T.W.N.; Bacon, S.; Bluhm, B.A.; Lique, C.; Melling, H.; Polyakov, I.V.; Straneo, F.; Timmermans, M.-L.; et al. Freshwater and Its Role in the Arctic Marine System: Sources, Disposition, Storage, Export, and Physical and Biogeochemical Consequences in the Arctic and Global Oceans. *J. Geophys. Res. Biogeosci.* **2016**, *121*, 675–717. [[CrossRef](#)]
6. Zhang, Y.; Chen, C.; Beardsley, R.C.; Gao, G.; Lai, Z.; Curry, B.; Lee, C.M.; Lin, H.; Qi, J.; Xu, Q. Studies of the Canadian Arctic Archipelago Water Transport and Its Relationship to Basin-local Forcings: Results from AO-FVCOM. *J. Geophys. Res. Ocean.* **2016**, *121*, 4392–4415. [[CrossRef](#)]
7. Onarheim, I.H.; Eldevik, T.; Smedsrud, L.H.; Stroeve, J.C. Seasonal and Regional Manifestation of Arctic Sea Ice Loss. *J. Clim.* **2018**, *31*, 4917–4932. [[CrossRef](#)]
8. Stroeve, J.C.; Kattsov, V.; Barrett, A.; Serreze, M.; Pavlova, T.; Holland, M.; Meier, W.N. Trends in Arctic Sea Ice Extent from CMIP5, CMIP3 and Observations. *Geophys. Res. Lett.* **2012**, *39*, 2012GL052676. [[CrossRef](#)]
9. Kwok, R. Arctic Sea Ice Thickness, Volume, and Multiyear Ice Coverage: Losses and Coupled Variability (1958–2018). *Environ. Res. Lett.* **2018**, *13*, 105005. [[CrossRef](#)]
10. Olason, E.; Notz, D. Drivers of Variability in Arctic Sea-ice Drift Speed. *J. Geophys. Res. Ocean.* **2014**, *119*, 5755–5775. [[CrossRef](#)]
11. Wang, K.; Zhang, Y.; Chen, C.; Song, S.; Chen, Y. Impacts of Arctic Sea Fog on the Change of Route Planning and Navigational Efficiency in the Northeast Passage during the First Two Decades of the 21st Century. *J. Mar. Sci. Eng.* **2023**, *11*, 2149. [[CrossRef](#)]
12. Zhang, Y.; Sun, X.; Zha, Y.; Wang, K.; Chen, C. Changing Arctic Northern Sea Route and Transpolar Sea Route: A Prediction of Route Changes and Navigation Potential before Mid-21st Century. *J. Mar. Sci. Eng.* **2023**, *11*, 2340. [[CrossRef](#)]
13. Shen, X.; Zhang, Y.; Chen, C.; Hu, S.; Xu, D.; Shao, W.; Chang, L.; Feng, G. Arctic Sea Ice Variation in the Northwest Passage in 1979–2017 and Its Response to Surface Thermodynamics Factors. *Adv. Clim. Change Res.* **2021**, *12*, 563–580. [[CrossRef](#)]
14. Zhang, Y.; Chen, C.; Beardsley, R.C.; Gao, G.; Qi, J.; Lin, H. Seasonal and Interannual Variability of the Arctic Sea Ice: A Comparison between AO-FVCOM and Observations: Numerical Study on the Arctic Sea Ice. *J. Geophys. Res. Ocean.* **2016**, *121*, 8320–8350. [[CrossRef](#)]
15. Johnson, M.; Proshutinsky, A.; Aksenov, Y.; Nguyen, A.T.; Lindsay, R.; Haas, C.; Zhang, J.; Diansky, N.; Kwok, R.; Maslowski, W.; et al. Evaluation of Arctic Sea Ice Thickness Simulated by Arctic Ocean Model Intercomparison Project Models. *J. Geophys. Res. Ocean.* **2012**, *117*, 2011JC007257. [[CrossRef](#)]
16. Kurtz, N.T.; Farrell, S.L.; Studinger, M.; Galin, N.; Harbeck, J.P.; Lindsay, R.; Onana, V.D.; Panzer, B.; Sonntag, J.G. Sea Ice Thickness, Freeboard, and Snow Depth Products from Operation IceBridge Airborne Data. *Cryosphere* **2013**, *7*, 1035–1056. [[CrossRef](#)]
17. Haas, C.; Lobach, J.; Hendricks, S.; Rabenstein, L.; Pfaffling, A. Helicopter-Borne Measurements of Sea Ice Thickness, Using a Small and Lightweight, Digital EM System. *J. Appl. Geophys.* **2009**, *67*, 234–241. [[CrossRef](#)]
18. Richter-Menge, J.A.; Perovich, D.K.; Elder, B.C.; Claffey, K.; Rigor, I.; Ortmeier, M. Ice Mass-Balance Buoys: A Tool for Measuring and Attributing Changes in the Thickness of the Arctic Sea-Ice Cover. *Ann. Glaciol.* **2006**, *44*, 205–210. [[CrossRef](#)]
19. Bi, H.; Zhang, J.; Wang, Y.; Zhang, Z.; Zhang, Y.; Fu, M.; Huang, H.; Xu, X. Arctic Sea Ice Volume Changes in Terms of Age as Revealed From Satellite Observations. *IEEE J. Sel. Top. Appl. Earth Obs. Remote Sens.* **2018**, *11*, 2223–2237. [[CrossRef](#)]
20. Kwok, R.; Cunningham, G.F. Variability of Arctic Sea Ice Thickness and Volume from CryoSat-2. *Philos. Trans. R. Soc. Math. Phys. Eng. Sci.* **2015**, *373*, 20140157. [[CrossRef](#)]
21. Zwally, H.J.; Schutz, B.; Abdalati, W.; Abshire, J.; Bentley, C.; Brenner, A.; Bufton, J.; Dezio, J.; Hancock, D.; Harding, D.; et al. ICESat’s Laser Measurements of Polar Ice, Atmosphere, Ocean, and Land. *J. Geodyn.* **2002**, *34*, 405–445. [[CrossRef](#)]
22. Laxon, S.W.; Giles, K.A.; Ridout, A.L.; Wingham, D.J.; Willatt, R.; Cullen, R.; Kwok, R.; Schweiger, A.; Zhang, J.; Haas, C.; et al. CryoSat-2 Estimates of Arctic Sea Ice Thickness and Volume: CRYOSAT-2 Sea Ice Thickness and Volume. *Geophys. Res. Lett.* **2013**, *40*, 732–737. [[CrossRef](#)]
23. Mecklenburg, S.; Drusch, M.; Kerr, Y.H.; Font, J.; Martin-Neira, M.; Delwart, S.; Buenadicha, G.; Reul, N.; Daganzo-Eusebio, E.; Oliva, R.; et al. ESA’s Soil Moisture and Ocean Salinity Mission: Mission Performance and Operations. *IEEE Trans. Geosci. Remote Sens.* **2012**, *50*, 1354–1366. [[CrossRef](#)]
24. Ricker, R.; Hendricks, S.; Kaleschke, L.; Tian-Kunze, X.; King, J.; Haas, C. A Weekly Arctic Sea-Ice Thickness Data Record from Merged CryoSat-2 and SMOS Satellite Data. *Cryosphere* **2017**, *11*, 1607–1623. [[CrossRef](#)]
25. Markus, T.; Neumann, T.; Martino, A.; Abdalati, W.; Brunt, K.; Csatho, B.; Farrell, S.; Fricker, H.; Gardner, A.; Harding, D.; et al. The Ice, Cloud, and Land Elevation Satellite-2 (ICESat-2): Science Requirements, Concept, and Implementation. *Remote Sens. Environ.* **2017**, *190*, 260–273. [[CrossRef](#)]
26. Wang, X.; Key, J.; Kwok, R.; Zhang, J. Comparison of Arctic Sea Ice Thickness from Satellites, Aircraft, and PIOMAS Data. *Remote Sens.* **2016**, *8*, 713. [[CrossRef](#)]
27. Li, M.; Ke, C.-Q.; Xie, H.; Miao, X.; Shen, X.; Xia, W. Arctic Sea Ice Thickness Retrievals from CryoSat-2: Seasonal and Interannual Comparisons of Three Different Products. *Int. J. Remote Sens.* **2020**, *41*, 152–170. [[CrossRef](#)]

28. Sallila, H.; Farrell, S.L.; McCurry, J.; Rinne, E. Assessment of Contemporary Satellite Sea Ice Thickness Products for Arctic Sea Ice. *Cryosphere* **2019**, *13*, 1187–1213. [[CrossRef](#)]
29. Tian-Kunze, X.; Kaleschke, L.; Maaß, N.; Mäkynen, M.; Serra, N.; Drusch, M.; Krumpfen, T. SMOS-Derived Thin Sea Ice Thickness: Algorithm Baseline, Product Specifications and Initial Verification. *Cryosphere* **2014**, *8*, 997–1018. [[CrossRef](#)]
30. Petty, A.A.; Kurtz, N.; Kwok, R.; Markus, T.; Neumann, T.A.; Keeney, N. *ICESat-2 L4 Monthly Gridded Sea Ice Thickness, Version 3*; NASA National Snow and Ice Data Center Distributed Active Archive Center: Boulder, CO, USA, 2023. [[CrossRef](#)]
31. Hendricks, S.; Paul, S. *Product User Guide & Algorithm Specification—AWI CryoSat-2 Sea Ice Thickness, version 2.6*; Zenodo: Genève, Switzerland, 2023. [[CrossRef](#)]
32. Kurtz, N.; Studinger, M.; Harbeck, J.; Onana, V.; Yi, D. *IceBridge Sea Ice Freeboard, Snow Depth, and Thickness Quick Look, Version 1*; NASA National Snow and Ice Data Center Distributed Archive Center: Boulder, CO, USA, 2022. [[CrossRef](#)]
33. Jutila, A.; Hendricks, S.; Ricker, R.; von Albedyll, L.; Haas, C. *Airborne Sea Ice Parameters during the IceBird Winter 2019 Campaign in the Arctic Ocean, version 1*; PANGAEA: Bremerhaven, Germany, 2021. [[CrossRef](#)]
34. Krishfield, R.A.; Proshutinsky, A. *BGOS ULS Data Processing Procedure*; Woods Hole Oceanographic Institute: Woods Hole, MA, USA, 2006; Available online: <https://www.whoi.edu/fileserver.do?id=85684&pt=2&p=100409> (accessed on 22 December 2022).
35. Wingham, D.J.; Francis, C.R.; Baker, S.; Bouzinac, C.; Brockley, D.; Cullen, R.; De Chateau-Thierry, P.; Laxon, S.W.; Mallow, U.; Mavrocordatos, C.; et al. CryoSat: A Mission to Determine the Fluctuations in Earth’s Land and Marine Ice Fields. *Adv. Space Res.* **2006**, *37*, 841–871. [[CrossRef](#)]
36. Jutila, A.; Hendricks, S.; Ricker, R.; von Albedyll, L.; Krumpfen, T.; Haas, C. Retrieval and Parameterisation of Sea-Ice Bulk Density from Airborne Multi-Sensor Measurements. *Cryosphere* **2022**, *16*, 259–275. [[CrossRef](#)]
37. Liston, G.E.; Itkin, P.; Stroeve, J.; Tschudi, M.; Stewart, J.S.; Pedersen, S.H.; Reinking, A.K.; Elder, K. A Lagrangian Snow-Evolution System for Sea-Ice Applications (SnowModel-LG): Part I—Model Description. *J. Geophys. Res. Ocean.* **2020**, *125*, e2019JC015913. [[CrossRef](#)] [[PubMed](#)]
38. Alexandrov, V.; Sandven, S.; Wahlin, J.; Johannessen, O.M. The Relation between Sea Ice Thickness and Freeboard in the Arctic. *Cryosphere* **2010**, *4*, 373–380. [[CrossRef](#)]
39. Kwok, R.; Kacimi, S.; Webster, M.A.; Kurtz, N.T.; Petty, A.A. Arctic Snow Depth and Sea Ice Thickness From ICESat-2 and CryoSat-2 Freeboards: A First Examination. *J. Geophys. Res. Ocean.* **2020**, *125*, e2019JC016008. [[CrossRef](#)]
40. Kacimi, S.; Kwok, R. Arctic Snow Depth, Ice Thickness, and Volume From ICESat-2 and CryoSat-2: 2018–2021. *Geophys. Res. Lett.* **2022**, *49*, e2021GL097448. [[CrossRef](#)]
41. Laxon, S.; Peacock, N.; Smith, D. High Interannual Variability of Sea Ice Thickness in the Arctic Region. *Nature* **2003**, *425*, 947–950. [[CrossRef](#)]
42. Zwally, H.J.; Yi, D.; Kwok, R.; Zhao, Y. ICESat Measurements of Sea Ice Freeboard and Estimates of Sea Ice Thickness in the Weddell Sea. *J. Geophys. Res.* **2008**, *113*, C02S15. [[CrossRef](#)]
43. Yi, D.; Zwally, H.J.; Robbins, J.W. ICESat Observations of Seasonal and Interannual Variations of Sea-Ice Freeboard and Estimated Thickness in the Weddell Sea, Antarctica (2003–2009). *Ann. Glaciol.* **2011**, *52*, 43–51. [[CrossRef](#)]
44. Kurtz, N.T.; Markus, T.; Cavalieri, D.J.; Sparling, L.C.; Krabill, W.B.; Gasiewski, A.J.; Sonntag, J.G. Estimation of Sea Ice Thickness Distributions through the Combination of Snow Depth and Satellite Laser Altimetry Data. *J. Geophys. Res.* **2009**, *114*, C10007. [[CrossRef](#)]
45. Hu, Z.; Chen, D.; Chen, X.; Zhou, Q.; Peng, Y.; Li, J.; Sang, Y. CCHZ-DISO: A Timely New Assessment System for Data Quality or Model Performance From Da Dao Zhi Jian. *Geophys. Res. Lett.* **2022**, *49*, e2022GL100681. [[CrossRef](#)]
46. Kern, S.; Ozsoy-Çiçek, B.; Worby, A. Antarctic Sea-Ice Thickness Retrieval from ICESat: Inter-Comparison of Different Approaches. *Remote Sens.* **2016**, *8*, 538. [[CrossRef](#)]
47. Nandan, V.; Geldsetzer, T.; Yackel, J.; Mahmud, M.; Scharien, R.; Howell, S.; King, J.; Ricker, R.; Else, B. Effect of Snow Salinity on CryoSat-2 Arctic First-Year Sea Ice Freeboard Measurements. *Geophys. Res. Lett.* **2017**, *44*, e2017GL074506. [[CrossRef](#)]

Disclaimer/Publisher’s Note: The statements, opinions and data contained in all publications are solely those of the individual author(s) and contributor(s) and not of MDPI and/or the editor(s). MDPI and/or the editor(s) disclaim responsibility for any injury to people or property resulting from any ideas, methods, instructions or products referred to in the content.